THESIS FOR THE DEGREE OF LICENTIATE OF ENGINEERING

# Modelling of laser plasma interaction with applications

BENJAMIN SVEDUNG WETTERVIK

Department of Physics

CHALMERS UNIVERSITY OF TECHNOLOGY

Gothenburg, Sweden 2018

Modelling of laser plasma interaction with applications

BENJAMIN SVEDUNG WETTERVIK



Department of Physics
Chalmers University of Technology
SE-412 96 Göteborg
Sweden
Tel: +46 (0) 31 772 1000

Printed in Sweden by
Reproservice
Chalmers Tekniska Högskola
Göteborg, Sweden, 2018

**Modelling of laser plasma interaction with applications**

Benjamin Svedung Wettervik
Department of Physics
Chalmers University of Technology

**Abstract**

The development of laser systems with ultra-high intensities has both opened up prospects for compact particle accelerators, as well as probing QED-effects, which are present in the high intensity regime. To describe laser matter interaction, it is necessary to self-consistently account for the paths of a large number of particles and the corresponding electromagnetic fields, with the addition of stochastic effects at high laser intensities. The primary method for modelling laser plasma interaction is the Particle-In-Cell (PIC) method, a Monte-Carlo method which samples phase-space with macro-particles and allows for efficient modelling of high dimensional problems. However, for some applications, for example shock acceleration and instability growth, continuum methods, i.e. solving the Vlasov-Maxwell system of equations on a phase-space grid, may be preferable to accurately describe the plasma dynamics. In the first two papers in this thesis, we adress the problem of implementing efficient continuum methods for the Vlasov-Maxwell system of equations. Furthermore, we treat ion shock acceleration using continuum methods.

This thesis also contains an investigation of the prospects for driving electron wakefield acceleration using coherent X-ray pulses. Recent advances in the theory for generation of high harmonics indicate the feasibility of relativistic amplitude coherent X-ray pulses, which could be used to drive a wakefield in a solid density plasma. We show by PIC-simulations, incorporating QED-effects, that similarity scaling laws hold for $\lambda = 5\,\mathrm{nm}$ and moderate relativistic amplitudes $a_0 \sim 10 - 100$. The quantum parameter $\chi$ is shown to be enhanced, leading to comparable electron and photon energies already at moderate $a_0 \sim 50$ although with more infrequent emission of photons than at optical wavelengths, preventing radiation losses from becoming a roadblock for the acceleration process.

**Keywords:** plasma, Vlasov-Maxwell equations, continuum methods, ion acceleration, coherent X-ray pulses, electron wakefield acceleration, radiation generation

# Publications

**A** B. Svedung Wettervik, T. C. DuBois and T. Fülöp,
*Vlasov modelling of laser-driven collisionless shock acceleration of protons,*
Physics of Plasmas 23, 053103, 2016.
arXiv:1512.06644 [physics.plasm-ph]

**B** B. Svedung Wettervik, T. C. DuBois, E. Siminos and T. Fülöp,
*Relativistic Vlasov-Maxwell modelling using finite volumes and adaptive mesh refinement,*
The European Physical Journal D 71 (6), 157, 2017.
arXiv:1606.08681 [physics.plasm-ph]

**C** B. Svedung Wettervik, A. Gonoskov, and M. Marklund,
*Prospects and limitations of wakefield acceleration in solids,*
Physics of Plasmas 25, 013107, 2018.
arXiv:1709.02190 [physics.plasm-ph]

Other publications, not included in the thesis:

**D**

E. Siminos, M. Grech, B. Svedung Wettervik and T. Fülöp,
*Kinetic and finite ion mass effects on the transition to relativistic self-induced transparency in laser-driven ion acceleration,*
New Journal of Physics 19 (12), 123042, 2017.
arXiv:1603.06436 [physics.plasm-ph]

# Contents

## Acknowledgements

I am grateful to my supervisor Mattias Marklund, and to Arkady Gonoskov for always being supporting and providing guidance in the endeavours which constitute this thesis. Furthermore, throughout this project I have had the opportunity to work with several excellent people contributing to a creative and friendly work environment. In addition to the people already mentioned, I would like to recognize Tim Dubois, Tünde Fülöp and Evangelos Siminos for good collaboration in projects, as well as Joel Magnusson and Stefan Buller for providing occasional distractions from the tasks needed to be done. Finally, I would like to extend my gratitude to my family, especially my girlfriend Qian Wang, for making every step along the path to this thesis a happy moment.

Benjamin Svedung Wettervik, 2018

# Chapter 1

# Introduction

The topic of this thesis is the interaction of high intensity laser light with plasma and some of its applications to particle acceleration. This field has been sparked by the fast development in laser technology since the realisation of the first laser by Maiman in the year 1960 [1]. These advances can be attributed to the development of Chirped Pulse Amplification [2] (CPA), which allows to temporally stretch the pulse and hence make it possible to reach high intensities without destroying the laser optics. Contemporary laser systems can reach intensities up to $I \sim 10^{22}\,\mathrm{W/cm^2}$, which is higher than focusing all sun light reaching the face of the earth to an area similar to the tip of a hair. There is today a multitude of high intensity laser facilities [3, 4, 5]. The extreme intensities have created interest for a number of applications of high intensity lasers, of which compact particle accelerators is one, realised by letting the laser irradiate ionised matter – plasma.

As laser plasma interaction is strongly nonlinear, numerical methods are necessary to assist the understanding from analytical models and in detail describe the properties of laser plasma interaction. However, adapting a single-particle picture and numerically accounting for the paths of all particles is well beyond existing and foreseeable computing resources. Instead, all computational models need to resort to some sort of approximation, for example as in kinetic or fluid models. Kinetic models are necessary for problems where the velocity distribution of the plasma particles is essential, which is often the case. The Particle-In-Cell (PIC) method [6, 7] is nowadays a standard tool for kinetic modelling of laser plasma interaction. In this method, the single particles are sampled and a limited number of macro-particles are tracked, whose paths are

calculated, with the electromagnetic fields self-consistently advanced on a grid for the spatial dimensions. The PIC-method has also been successful to incorporate QED effects, as the stochastic event of emission of a photon or creation of an electron-positron pair relies on that the particle picture to some extent is maintained. This is of interest for modelling prospective experiments in next generation laser facilities, e.g. the Extreme Light Infrastructure (ELI) [8].

One of the foremost strengths of the PIC-method – that it samples velocity space – is also a shortcoming for a limited range of applications where a detailed noise-free description of velocity space is critical. This is also the case for problems where collisional processes are important. For these problems, continuum methods need to be used, which discretise the distribution function and solve the Vlasov-Maxwell system of equations on a phase space grid [9]. However, the use of a grid incorporating the velocity dimensions comes at the disadvantage that the problem becomes computationally more demanding. Solvers for the Vlasov-Maxwell system are therefore primarily used when it is possible to consider a model with reduced dimensionality. In this thesis, some attention is paid to the development of efficient Vlasov-Maxwell solvers, e.g. utilising an adaptive grid, to reduce the computational costs.

Since the 1990s, the development of high intensity lasers has opened up the possibilities for laser plasma accelerators. For electron acceleration, lasers can be used to drive plasma waves moving close to the speed of light, trapping and accelerating electrons [10]. This is known as wakefield acceleration and has been demonstrated to provide high quality electron beams of several GeV [11]. Whereas contemporary wakefields are driven by optical wavelength lasers (or particle beams), in this thesis, we treat the effects of using an X-ray pulse to drive the wake.

For ion acceleration, the high mass of ions prevent trapping in moving structures with velocities close to the speed of light and different approaches must be adopted. The laser field needs to be converted into a slow-moving field structure to allow for acceleration. With the first mentioning of plasma based ion accelerators in 1957 by Veksler [12], several laser-plasma based techniques for ion acceleration have today been devised. Target Normal Sheet Acceleration (TNSA) is one of the most studied schemes [13, 14]. Whereas TNSA is very robust and can have a high conversion efficiency of laser energy into energy of the plasma particles, the acceleration process leads to ions with a thermal spectrum. Other methods, for example shock acceleration where ions are reflected

by a moving potential barrier can provide a mono-energetic spectrum, which is beneficial for applications. However, the conversion of laser energy into ion energy is less efficient and obtaining a significant number of accelerated particles is challenging. Continuum methods are beneficial for modelling shocks, which therefore are considered in connection to the continuum solvers that are implemented as a part of this work.

### Outline

This thesis is organised as follows: In Chapter 2, we define the plasma state and formulate the governing equations. This is followed by Chapter 3, which gives an introduction to some aspects of electron wakefield acceleration and shock driven ion acceleration, which is treated in Papers A and C. In Chapter 4, the PIC-method is discussed, as well as compared with continuum methods for the Vlasov-Maxwell system, connecting to Papers A and B. Finally, Chapter 5 gives an overview of the papers that are included in this thesis, as well as the contribution by the author.

# Chapter 2

# The equations of plasma physics

A plasma is defined as a quasi-neutral ionized gas which exhibits collective behaviour, i.e. a state which consists of freely moving charges: electrons, ions and potentially positrons, that interact through long range electromagnetic fields. This is different from ordinary matter, such as solids, liquids and gases, where short range interactions between nearest neighbours play a more important role. A more quantitative understanding of the definition of a plasma can be obtained by considering the effect of a small test charge, with charge $q$, in a plasma with background density $n_0$. The plasma then sets up a density perturbation and potential $\phi$ described by:

$$n_e = n_0 \exp(e\phi/k_B T) \quad \text{and} \quad \phi = \frac{q}{r} \exp(-r/\lambda_D)$$

where $k_B$ is the Boltzmann constant, $T$ the temperature of the electrons, $e$ the elementary charge and $\lambda_D$ is the Debye length, defined by:

$$\lambda_D = \sqrt{\frac{k_B T}{4\pi n_0 e^2}}.$$

The potential should be compared to the Coulomb potential of the particle: $q/r$. It is clear that the plasma acts to shield the effects of individual charges with a characteristic scale of $\lambda_D$. This model breaks down if $\lambda_D$ is too small compared to the average particle distance. The conditions for quasi-neutrality and dominance of collective effects can hence be expressed in terms of $n_0 \lambda_D^3 \gg 1$, i.e. that a volume with dimensions of the Debye length must contain many particles.

In the field of laser plasma interaction, a laser pulse is commonly incident on a plasma-vacuum surface. The character of the dynamics depends on a number of factors, e.g. the amplitude, shape and duration of the pulse, as well as the plasma profile and density. The relativistic amplitude of a laser pulse, defined by $a_0 = eE_{\max}/m_e c\omega$, where $c$ is the speed of light, $m_e$ is the electron mass, $\omega$ is the angular frequency of the laser and $E_{\max}$ is the maximum electromagnetic field strength, is an important scale for the degree of relativistic motion in the interaction. It defines a typical energy scale: $\epsilon = m_e c^2(\gamma - 1) \approx a_0 m_e c^2$ ($\gamma$ is the gamma factor) for electrons interacting with the laser field.

To describe the plasma dynamics, it is necessary to self-consistently account for the dynamics of all plasma particles and the electromagnetic fields [15]. This can, for a classical plasma, be done by solving the equations of motion of the particles:

$$\frac{\partial \vec{r}_i(t)}{\partial t} = \vec{p}_i(t)$$
$$\frac{\partial \vec{p}_i(t)}{\partial t} = q_s(\vec{E} + \vec{v}_i(t) \times \vec{B}/c),$$

where $\vec{r}_i(t)$, $\vec{p}_i(t)$ denotes the position and momentum vectors of particle $i$, $\vec{v}_i(t) = \vec{p}_i(t)/(\gamma m_s)$ is its velocity and $m_s$, $q_s$ are its mass as well as charge.

$$\vec{F}_L = q_s(\vec{E} + \vec{v}_i(t) \times \vec{B}/c)$$

is the Lorentz force. $\vec{E}$ and $\vec{B}$ are the electromagnetic fields satisfying Maxwells equations [16], defined by:

$$\nabla \cdot \vec{E} = 4\pi\rho$$
$$\nabla \times \vec{E} = -\frac{1}{c}\frac{\partial \vec{B}}{\partial \vec{x}}$$
$$\nabla \cdot \vec{B} = 0$$
$$\nabla \times \vec{B} = \frac{4\pi}{c}\vec{J} + \frac{1}{c}\frac{\partial \vec{E}}{\partial t}.$$

Here, $\vec{J}$ and $\rho$ is the current and charge density, respectively.

Although the many degrees of freedom in the single-particle image provides a full picture, it does in most situations become too complicated to be used to gain substantial insights in the dynamics of the plasma. A more coarse grained description of the plasma dynamics is obtained by noticing that the large number of particles allow the use of statistical

methods, introducing a distribution function $f_s(\vec{x},\vec{p},t)$, where $s$ is an index for the species and $\vec{x}$, $\vec{p}$ are position and momentum coordinates for a six dimensional phase space. This distribution function describes the number of particles $dN = f_s(\vec{x},\vec{p},t)\mathrm{d}^3\vec{x}\mathrm{d}^3\vec{p}$ in a phase-space volume $\mathrm{d}^3\vec{x}\mathrm{d}^3\vec{p}$. For collisionless plasma, the distribution function satisfies a continuity equation known as the Vlasov-equation [17, 18]:

$$\frac{\partial f_s}{\partial t} + \frac{p_i}{m_s\gamma_s}\frac{\partial f}{\partial x_i} + q_s\left[E_i + \frac{1}{\gamma m_s}(\vec{p}\times\vec{B})_i\right]\frac{\partial f}{\partial p_i} = 0$$

with $\gamma = \sqrt{p^2/m^2c^2+1}$. Using the distribution function, the charge and current densities can be expressed as:

$$\vec{J} = \sum_s \frac{q_s}{m_s}\int \frac{\vec{p}}{\gamma_s} f_s \,\mathrm{d}^3p$$

and

$$\rho = \sum_s q_s \int f_s \,\mathrm{d}^3p,$$

where the summation ranges over all species $s$ in the plasma.

In the derivation of the Vlasov equation, the transition from the particle description to the distribution $f_s(\vec{x},\vec{p},t)$ is performed through an averaging process. As a consequence, detailed information about the field structure is transferred into a collision term. The collision term has contributions from the interactions between the individual particles, typically modelled as binary interactions. Because of the short time scale of a collisional event, it can be modelled by a cross-section leading to a disruptive change of the particle momenta. In fusion energy, collisional processes are of paramount importance. However, in laser-plasma physics: the typical time scale of plasma dynamics is defined by the laser period and is short compared to the average time between collisional events. This can be indicated by estimating the (electron-ion) collision frequency for relativistic electrons: $v_{ei} = 4\pi n_e Z c r_0^2 \log\Lambda/\gamma^2$, where $Z$ is the charge number for ions, $\log\Lambda$ is the Coulomb logarithm and $r_0$ is the classical electron radius. Taking typical values $\log\Lambda \sim 10$, $Z \sim 10$ and $\gamma \sim a_0$, assuming $a_0 \sim 10$ for contemporary laser facilities, the collision frequency is $v_{ei} = 3\cdot 10^{-18} n_e$. Typical densities for plasmas range from $n_e = 10^{18}\,\mathrm{cm}^{-3}$ to $10^{24}\,\mathrm{cm}^{-3}$ for gas jets and solids respectively. Consequently $v_{ei}$ ranges between 3 Hz to 3 MHz, which can be compared to the laser frequency $f = 300\,\mathrm{THz}$ for optical wavelengths

($\lambda = 1\,\mu$m). Furthermore, as the collision frequency decrease with the electron energy, collisional effects are less important for particle beams reaching high energies, e.g. electron beams in wakefield acceleration.

In Papers A and B, we consider a Vlasov-equation of reduced dimensionality, with only one spatial ($x$) and momentum ($p_x$) direction respectively. For a problem where the transverse variations in the laser and plasma density (with respect to the propagation direction $x$) are small, the Hamiltonian for a plasma particle is:

$$H = m_s c^2 \left[ 1 + \frac{(\vec{\Pi}_s - q_s \vec{A})^2}{m_s^2 c^2} \right]^{1/2} + q_s \phi$$

and only depends on $x$. Here, $\vec{A}$ is the electrostatic vector potential, defined by $\vec{B} = \nabla \times \vec{A}$. This yields conservation relations for the transverse canonical momentum: $\Pi_{s\perp} = q_s A_\perp + p_\perp = 0$, which can be used to calculate the $\gamma$ factor. One dimensional models are also applicable in cases where a laser impinges on a surface at an oblique angle (by using a Lorentz transformation).

## 2.1 Radiation reaction and QED effects

In the classical picture, electromagnetic waves are radiated from accelerated charges. In contrast to this description in terms of fields, quantum electrodynamics (QED) dictates that light is mediated by particles, more precisely photons, and that radiation can be interpreted as the emission of these particles. The description in terms of photons is necessary to capture the incoherent radiation from high energy particles. The energy of an emitted photon; $E = \hbar\omega_r$, where $\hbar$ is the Planck constant and $\omega_r$ the angular frequency of the photon, is equal to the energy lost by the radiating particle. The dominant contribution comes from synchrotron radiation, which is due to acceleration transverse to the particle velocity. For relativistic particles, synchrotron radiation results in photon emission with a typical frequency:

$$\omega_r = \frac{3}{2}\omega_0 \gamma^3$$

where $\omega_0$ is the non-relativistic synchrotron frequency. Hence; particles with small mass, which can gain large relativistic factors $\gamma$ by interacting with the laser field, i.e. electrons and potentially also positrons,

are responsible for radiation of high energy photons. It is evident that the energy of the emitted photons grows quickly with the intensity of the laser ($\omega_r \sim a_0^3$) and can for relativistically intense laser pulses be significantly higher than the frequency of the laser radiation $\omega$.

The character of the radiation is determined by the value of the dimensionless parameter:

$$\chi = \gamma E_\perp / E_c$$

where $\gamma$ is the gamma-factor of a radiating particle, $E_\perp$ is the transverse electric field experienced by the particle and $E_c = m_e^2 c^3 / e\hbar$ is the Schwinger field. In the classical regime, for which $\chi \ll 1$, $\chi$ is proportional to the ratio between the energy of a typical emitted photon and radiating particle: $2\hbar\omega_c / 3\gamma m_e c^2$. For $\chi \ll 1$, since the fraction of the energy of the radiating particle and emitted photon energy is small, the emission of radiation only affects the particle dynamics if emission events are frequent. In that case, the effect on the particle dynamics can be described by a continuous force, e.g. the Landau-Lifschitz force [19], which to leading order takes the form:

$$\vec{f} = -\frac{2}{3}\frac{e^2 m^2 c}{\hbar^2}\chi^2 \vec{v}$$

where $\vec{v}$ is the velocity of the particle.

The classical treatment using a continuous force for the effect of radiation on the emitting particle, known as radiation reaction, is only valid for $\chi \ll 1$. As $\chi$ approaches one, the energies of the photons become similar to those of the emitting particles, leading to recoils which significantly alter the paths of the emitting particles. In this case, it is necessary to describe the radiation in terms of probabilities and cross-sections from QED [20]. The probability distribution for an emission event during an infinitesimal time $\Delta t$ is given by:

$$\frac{\mathrm{d}P}{\mathrm{d}\delta} = \left[\Delta t \frac{e^2 m_e c}{\hbar^2}\right] \frac{\sqrt{3}}{2\pi}\frac{\chi}{\gamma}\frac{1-\delta}{\delta}\left\{F_1(z_q) + \frac{3}{2}\delta\chi z_q F_2(z_q)\right\}$$

where $\delta$ is the photon to electron energy quotient, $z_q = 2\delta / 3\chi(1-\delta)$ and $F_1(x)$, $F_2(x)$ are the first and second synchrotron functions.

In qualitative terms, the effect of radiation reaction is determined by the energy distribution of the emitted photons in relation to those of the emitting particles and the frequency of emission events. When the intensity of the laser increases, both the typical energy fraction and emission

frequency is increased. For laser plasma interaction driven by optical laser pulses, and intensities where radiation reaction matters, emission events are frequent compared to the time-scale associated with plasma dynamics, which is the motivation for using a continuous force model. This is on the other hand not possible for scenarios with shorter wavelength pulses, for which emission events are infrequent also for moderate $\chi$. Compared to in the optical regime, this alters the electron dynamics by allowing the electrons to enter regions of space with higher field strengths, from which they would be shielded by the more frequent photon emission at optical wavelengths.

In Paper C, the effect of using nanometer wavelength pulses to drive wakefield acceleration is investigated, which is characterised by high values of $\chi$ but infrequent photon emissions, compared to at optical wavelengths.

# Chapter 3

# Some aspects of laser plasma interaction

## 3.1 Plasma waves and regimes of interaction

The ability of plasma to generate electromagnetic fields and self-organize accordingly leads to that plasma can sustain many different wave modes. A basic example is the so called Langmuir waves: If the density of an otherwise neutral plasma is perturbed, the plasma will oscillate about its non-perturbed state at a frequency:

$$\omega_p = \sqrt{\frac{4\pi n_e e^2}{m_e}},$$

which is known as the plasma frequency. If the electrons have a finite temperature $T_e$, the dispersion relation is modified: $\omega^2 = \omega_p^2 + 3k^2(k_B T_e/m_e)^2$, where $k$ is the magnitude of the wave-vector of the perturbation.

Electromagnetic waves are a different kind of waves, describing the propagation of electromagnetic fields in the presence of a plasma. Their dispersion relation is:

$$\omega^2 = \omega_p^2 + k^2 c^2$$

which in the limit of $\omega_p = 0$ (i.e. the plasma density is zero) coincides with the ordinary dispersion relation for light in vacuum.

Notice that the dispersion relation for electromagnetic waves has a lower frequency threshold $\omega_p$. It is consequently only possible for electromagnetic waves to propagate if their frequency $\omega$ is higher than

the plasma frequency $\omega_p$. Conversely, there is a critical (maximum) plasma density for which an electromagnetic wave with frequency $\omega$ can propagate in the plasma:

$$n_c = \frac{\omega^2 m_e}{4\pi e^2}.$$

If the laser pulse is strong enough to accelerate the electrons to relativistic energies, this threshold is modified by relativistic effects by replacing the electron mass with its relativistic counterpart $m_e\gamma$. Furthermore, this result applies for propagation of a wave that already is inside the plasma. If a laser pulse impinges on a vacuum plasma interface, the electrons reorganize themselves and the threshold for propagation is different. This will be discussed in Section 3.2. The threshold can be interpreted as the critical level of the density such that the current generated by electrons within the skin depth is large enough to counteract the incoming field.

The existence of a threshold density for propagation of light divides laser plasma interaction in two distinct regimes: An underdense regime where the density is below the threshold, hence allowing propagation of laser pulses, as well as an overdense regime in which the laser light is reflected and/or absorbed at the vacuum plasma interface. The waves excited by the laser pulse in the underdense regime move at a speed close to the speed of light, and this regime is therefore commonly used for electron acceleration. On the other hand, ions are more than a thousand times heavier than electrons and therefore respond more slowly to electromagnetic fields. This results in that they are not as efficiently accelerated by fast-moving plasma waves. Instead, ion acceleration often utilizes quasi-stationary fields which can be set up by interaction in the overdense regime.

## 3.2 The effect of vacuum plasma interface

For a stationary circularly polarized laser pulse incident on a vacuum plasma interface for a one-dimensional step-like overdense cold plasma, semi-analytical solutions exist for the stationary state reached by the plasma [21, 22, 23]. In Papers A and B, such solutions have been used to verify the correctness of implemented solvers for the Vlasov-Maxwell system. Under these circumstances, the cold fluid equations can be used. Assuming that $p_x = 0$ at an equilibrium, the cold fluid equations can be

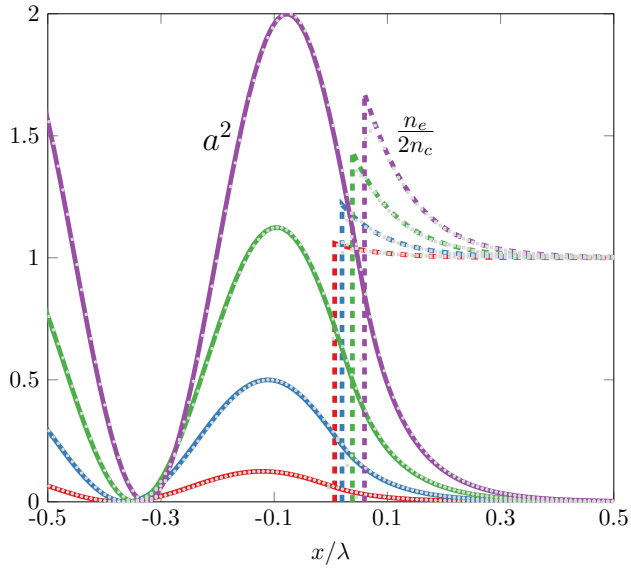


**Figure 3.1:** Plasma densities and vector potential for stationary solutions when a circularly polarized laser pulse impinges on a step-like plasma of initial density $2n_c$. The densities have been normalized by $2n_c$, to fit on the same scale as the squared vector potential. The analytical results for different intensities are labelled with the colours red ($a_0 = 0.25$), blue ($a_0 = 0.50$), green ($a_0 = 0.75$) and purple ($a_0 = 1.00$). Numerical results are coloured in grey.

written on the form:

$$\frac{\mathrm{d}\phi}{\mathrm{d}x} = \frac{\mathrm{d}\gamma}{\mathrm{d}x},$$

$$\frac{\mathrm{d}^2\phi}{\mathrm{d}x^2} = n_e - n_0,$$

$$\frac{\mathrm{d}^2 a}{\mathrm{d}x^2} = \left(\frac{n_e}{\gamma} - 1\right) a,$$

where $n_0$ is the unperturbed plasma density, $n_e$ is the electron density resulting from the interaction with the laser pulse, $\phi$ is a normalized electrostatic potential, $a$ is the vector potential and $\gamma = \sqrt{1 + a^2}$. Distance is expressed in terms of wavenumber and field strength in terms of the critical electric field.

For a circularly polarized pulse with amplitude $a_0$, the vacuum plasma surface is pushed by the pondermotive force leading to a pile up of electrons within a skin depth of the displaced vacuum plasma surface. In

the analytical theory, the surface is pushed up to a point $x_b$ at which the electrostatic force due to the displaced charge $q_e E_x$ is balanced by the pondermotive force $-m_e c^2 \partial\gamma/\partial x$. Denoting the value of the vector potential at this point by $a_b$, it holds that:

$$\frac{2a_0^2 + a_b^4}{1 + a_b^2} = 2n_0 \left( \sqrt{1 + a_b^2} - 1 \right).$$

The value of $a_b$ can be found from numerical calculation and $x_b$ can then be calculated by:

$$x_b = \frac{a_b}{n_0} \sqrt{\frac{2a_0^2 - a_b^2}{1 + a_b^2}}.$$

Based on these values for $x_b$ and $a_b$, the normalized vector potential in the vacuum and plasma regions become:

$$a(x) = \sqrt{2} a_0 \sin \left[ \arcsin \left( \frac{a_b}{\sqrt{2} a_0} \right) - (x - x_b) \right]$$

and

$$a(x) = \frac{2\sqrt{n_0(n_0 - 1)} \cosh[(x - x_0)/\lambda_s]}{n_0 \cosh[(x - x_0)/\lambda_s] - (n_0 - 1)},$$

respectively, where $\lambda_s = 1/\sqrt{n_0 - 1}$ is the skin depth and $x_0$ is determined by ensuring the continuity of the vector potential at $x = x_b$. The electron density is finally calculated from $n_e = n_0 + \partial^2\gamma/\partial x^2$.

In Figure 3.1: stationary analytical solutions as well as numerical solutions for the electron density and vector potential are shown for circularly polarized pulses of several different $a_0$ impinging on a plasma of density $n_e = 2n_c$ which initially is located at $x > 0$. In the numerical calculations, the solver in Paper B for the Vlasov-Maxwell system of equations was used. The plasma was assumed to initially have a Maxwellian distributions with a temperature $T_e \approx 0$ and the steady state is reached by interaction with a plane-wave with a rise time of four laser periods. For these parameters, the numerical solutions of the Vlasov-Maxwell system and those based on the semi-analytical formulas agree well. However, for higher field strengths $a_0$, ion motion effects and the finite rise time of the laser pulse may cause additional heating effects which alter the dynamics, especially for densities close to the critical density [24].

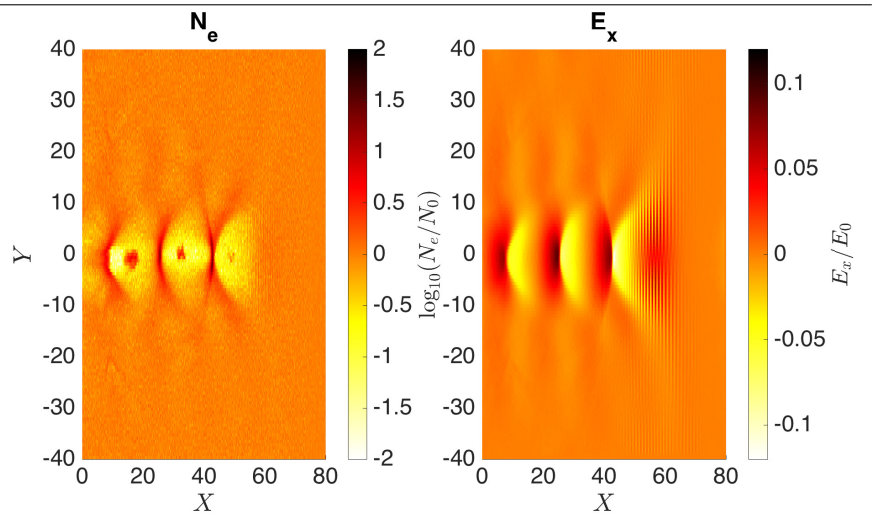


**Figure 3.2:** Electron density (left) and longitudinal electric field structure (right) for a wakefield in the bubble regime.

## 3.3 Electron wakefield acceleration

Laser-driven wakefield accelerators were first introduced by Tajima and Dawson [10], almost four decades ago. In an underdense plasma, an incoming laser pulse propagates at a velocity close to the speed of light and excites a plasma wave co-moving with the pulse. This gives rise to a potential structure moving at a high velocity. If an electron gains a sufficient momentum in the propagation direction of the pulse, it can be trapped in an accelerating phase by the potential structure, and reach high energies. In a one dimensional model, the minimum momentum needed for an electron to be trapped is given by $p_{x,i} = \gamma_p\beta(1+\gamma_p\Delta\phi) \pm \gamma_p\sqrt{(1+\gamma_p\Delta\phi)^2-1}$, where $\gamma_p = 1/\sqrt{1-\beta_p^2}$ is the gamma factor of the wake structure and $\Delta\phi$ is the size of the potential well.

Laser wakefield acceleration has been shown to accelerate electrons to GeV energies [11, 25, 26]. For non-relativistic pulses, defined by $a_0 \ll 1$, the excited wave and density perturbation has a sinusoidal dependence on the phase. If the intensity is increased, reaching a relativistic level $a_0 \sim$ 1-10, which is accessible with contemporary laser systems, non-linear wake structures where the laser expels all electrons – forming a bubble trailing after the laser pulse – occur. This regime of interaction

is known as the bubble regime and was discovered by Phukov *et al* [27]. Figure 3.2 shows electron densities and the longitudinal electric field for a wakefield in the bubble regime.

Laser-plasma interaction comprises a vast parameter space. To understand and optimize the physics it is therefore beneficial if a minimal number of parameters can be considered, from which the essential properties can be inferred. Consider a plasma with electron density $n_e$ interacting with a pulse propagating in the $x$-direction with vector potential of the form $\vec{a}(x,y,z,t) = a(r_\perp/R,(t-x/c)/\tau)\cos(\omega t - kx)\hat{z}$, where $r_\perp$ is the transverse radial coordinate, $R$ is the width of the pulse, $\tau$ is its duration and $k = \omega/c$ is the wave number. The interaction can be fully described by the four dimensionless parameters $kR$, $\omega\tau$, $n_e/n_c$ and $a_0$. For high $a_0$, the electrons become relativistic, moving at a speed close to the speed of light and the four dimensionless parameters can be reduced by combining $n_e/n_c$ and $a_0$ into the similarity parameter $S = n_e/a_0 n_c$, resulting in the three similarity parameters: $S$, $\hat{R} = S^{1/2}kR$ and $\hat{\tau} = S^{1/2}\omega\tau$ [27, 28]. The $S$ parameter can be viewed as a measure of how overdense the plasma is, incorporating relativistic effects. The reduction of $n_e/n_c$ and $a_0$ into the similarity parameter $S$ relies on that the velocity $\vec{v}$ can be approximated by $\vec{v}/c \approx \vec{p}/|\vec{p}|$, which holds if $(m/m_e a_0)^2 < 1$, where $m$ is the particle mass. This is the case electrons in the bubble regime, and the dynamics hence scales with the similarity parameter $S$.

## 3.4 QED effects in X-ray driven wakefield acceleration

The use of X-ray pulses instead of laser pulses with optical wavelengths to drive accelerating structures (in solid materials) was first suggested by Tajima *et al* in the 1980s [29]. The motivation for this can be derived from the similarity scaling relations which suggest that X-ray driven wakefield acceleration using solid density materials would allow much higher acceleration gradients than if optical wavelengths were used, as well as electron bunches whose temporal and spatial scales have been reduced proportionally to the wavelength. This is interesting for applications demanding extremely short bunches. The electron energies only scale with $a_0$ and are consequently independent of the wavelength.

In contrast to that the energies for accelerated electrons in the optical and X-ray driven regimes are the same, the radiation from the acceler-

ated electrons is widely different. The quantum parameter $\chi$ scales as $\chi \sim a_0^2(\lambda_c/\lambda)$, where $\lambda_c$ is the Compton wavelength. A reduction of the wavelength from $1\,\mu$m to 5 nm therefore results in an increase of the quantum parameter by a factor of 200. Hence, $\chi \sim 1$ already for $a_0 \sim 50$. In paper C, we investigate the effect of using coherent X-ray pulses to drive wakefield acceleration in the bubble regime, with intensities such that $\chi \sim 1$. This extends the intensity range considered in previous work using PIC-simulations [30] and is motivated by the theoretical development in generation of high harmonics, specifically the relativistic electron spring (RES) model [31, 32, 33, 34], which indicates the possibility to generate nanometer wavelength few cycle X-ray pulses with relativistic intensities.

The effect of the $\chi$ enhancement in the X-ray driven regime is to create a wakefield accelerator that emits photons at comparable energies to the electron energies, already at moderate $a_0$. However, this raises concerns regarding the role of radiation losses and if these will have a deteriorating effect on the accelerating process. Clearly, the discrete nature of photon emission will be crucial for describing the effect of the radiation. The wavelength effects on the radiation emission can be seen by expressing the pre-factor of the emission probability in terms of normalized coordinates: $\chi = \hat{\chi}\, a_0^2(\lambda_c/\lambda)$, $\gamma = a_0\hat{\gamma}$ and $\mathrm{d}t = T\mathrm{d}\hat{t}$:

$$\frac{\mathrm{d}P}{\mathrm{d}\delta} = \sqrt{3}a_0\,\Delta\hat{t}\,\frac{e^2}{c\hbar}\frac{\hat{\chi}}{\hat{\gamma}}\frac{1-\delta}{\delta}\left\{F_1(z_q) + \frac{3}{2}\delta\chi z_q F_2(z_q)\right\}.$$

It is natural to compare cases of an optical and X-ray driver having the same $\chi$ (i.e. different $a_0$). In that case, the emitted photons have the same spectrum normalized by the electron energy and the emission frequency is found to scale as $\sim\sqrt{\lambda}$. Using an X-ray pulse to operate a wakefield at a prescribed $\chi$ will hence result in fewer emitted photons per electron than at optical wavelengths. In summary, photon emission for a given $a_0$ leads energies closer to those of the electrons, but with a frequency that is smaller in comparison to the laser period than for an optically driven wakefield with the same shape of the spectral distribution.

## 3.5 Shock acceleration

Paper A treats laser driven shock acceleration of ions. A shock is defined as a propagating structure which changes the macroscopic state over a

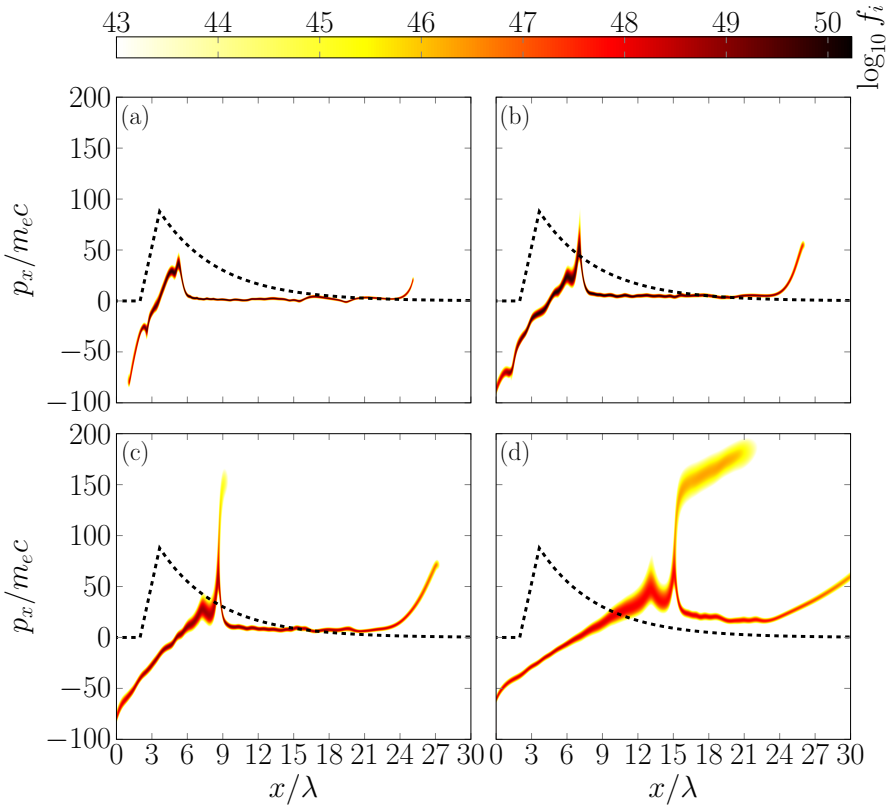


**Figure 3.3:** Ion distribution function at consecutive instants of time (a to d) for a near critical density plasma interacting with a linearly polarized laser pulse. The initial plasma density has been indicated by black dashed lines.

transition layer. Shock waves can be driven by laser pulses interacting with near critical plasmas: The radiation pressure from the pulse leads to a pile up of electrons on the laser plasma interface, which is pushed to high speed. This leads to the formation of an electrostatic potential structure which continues to travel into the plasma even after the laser pulse has finished interacting with the plasma. The electrostatic structure travels at a velocity $v_s$ (known as the shock-velocity), which in many cases is close to the hole-boring velocity:

$$v_{\mathrm{HB}} = a_0 c \left[(Z/A)(m_e/m_p)(n_c/n_e)(1+R)/2\right]^{1/2},$$

where $Z$, $A$ are the charge and mass numbers for the ions and $R$ is the reflectivity of the plasma surface. The symmetry of the up- and down-stream region is broken if the potential is high enough to reflect a fraction of the bulk ions. In the frame of the moving potential structure, the ions are moving at a speed $-v_s$ and are consequently reflected to a speed $2v_s$ in a frame at rest. Provided that the shock only reflects a small fraction of the ions, shock acceleration provides a monoenergetic ion bunch. Figure 3.3 shows a distribution function for ions, with reflected ions, for a shock driven by a linearly polarized laser pulse. Finally, by having a smoothly decaying density down ramp it is possible to maintain the monoeneregetic spectrum of the ions when they exit the plasma [36].

As indicated, the process of laser driven ion shock acceleration contains several steps of energy conversion: First a transfer from the laser to the electrons, followed by that part of the electron energy is converted into the electrostatic potential structure moving at the speed $v_s$. Finally, the energy in the potential structure is converted to ion energy through the reflection process. Efficient realization of shock acceleration therefore builds on optimization of several individual steps, which may be complicated. However, since shock reflection leads to a monoenergetic spectrum, getting enough ions within a specific energy range put weaker conditions on the conversion efficiency than for methods providing a thermal spectrum. A basic description of ion acceleration using electrostatic shocks is given by Moiseev *et al* [37], which is based on a fluid description for the ions which manually takes the reflected ions into account.

In this model, the electron density is assumed to follow a Boltzmann distribution:

$$n_e = n_0 \exp(e\phi/k_B T_e)$$

where $n_0$ is the background density, $T_e$ is the electron temperature and $\phi$ is the electrostatic potential. The ion density $n_i$ and velocity $v_i$ satisfy the fluid equations:

$$m_i \left( \frac{\partial v_i}{\partial t} + v_i \frac{\partial v_i}{\partial x} \right) = -e \frac{\partial \phi}{\partial x},$$

$$\frac{\partial n_i}{\partial t} + \frac{\partial (n_i v_i)}{\partial x} = 0$$

combined with a Poisson equation:

$$-\frac{\partial^2 \phi}{\partial x^2} = 4\pi e (n_i - n_0 \exp(e\phi/k_B T_e))$$

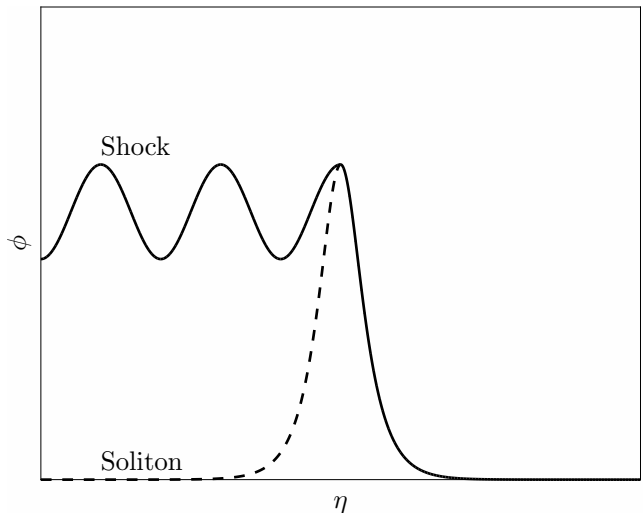


**Figure 3.4:** Shock and soliton potential structure.

for the potential. It is assumed that all quantities are stationary in a frame moving with the shock velocity, described by the coordinate $\eta = x - v_s t$. These equations can then be transformed into:

$$\frac{\partial^2 \phi}{\partial \eta^2} = 4\pi n_0 e \left( \frac{v_s}{\sqrt{v_s^2 - 2e\phi/m_i}} - \exp(e\phi/T_e) \right) \tag{3.1}$$

where the right hand side can be expressed as $-\frac{\partial V(\phi)}{\partial \phi}$. $V(\phi)$ is an effective potential taking the form:

$$V(\phi) = 4\pi n_0 \left( m_i v_s \sqrt{v_s^2 - 2e\phi/m_i} + k_B T_e \exp(e\phi/k_B T_e) \right).$$

Consequently, the potential satisfies $(\partial_\eta \phi)^2 + V(\phi) = C$ for some constant value $C$ and $\phi$ can be interpreted as the position of a particle moving in the potential $V(\phi)$, with $\eta$ taking the role of a time coordinate. Up to this point, the model does not incorporate the effect of reflected ions and is therefore only valid for low enough potential barriers, defined by $\phi << v_s^2 m_i/2e$. The solution to (3.1) is symmetric around a maxima of the potential at $\eta = 0$ and the fluid state is left unperturbed after interacting with the potential barrier passing through. This type of solution is known as a solitary wave. For a solitary wave, ions are not accelerated. On the contrary, in a shock wave: the symmetry around

$\eta = 0$ is broken by reflection of ions. This occurs when the height of the potential barrier starts to approach $v_s^2 m_i/2e$. The fraction of reflected ions for a potential barrier of height $\phi$ can be defined as:

$$F(\phi) = \int_{m_i(v_s+v_x)^2/2<e\phi} f_i(v_x)\mathrm{d}v_x$$

and modifies the Poisson equation in the up- and down-stream regions respectively. This leads to a different potential structure in the up- and down-stream region and breaks the symmetry of the potential around $\eta = 0$. Figure 3.4 schematically shows the potential in the soliton and shock cases respectively. For steady shock acceleration, the fraction of reflected ions can not be too big as it leads to a quick transfer of the energy in the potential structure to the ions, and consequently a decay of the accelerating field structure. To model shock acceleration it is hence necessary to accurately resolve the low density tail of the ion distribution. Continuum methods are suitable as they can resolve the low density tail of the ion distribution with low levels of numerical noise.

As a summary, the benefit of shock acceleration is that the reflection process leads to monoenergetic ions inside the plasma. However, a challenge is how to robustly control the number of ions and achieving a high enough number to be useful for applications.

# Chapter 4

# Numerical methods

The Particle-In-Cell method [6] is the most widely used method for kinetic simulations of laser plasma interaction. In this method, the plasma is modelled as an ensemble of particles which is advanced self-consistently with the electromagnetic fields. Consequently, the PIC-method uses a grid for the spatial dimensions of the setup, to represent the fields, but not for the momentum space dimensions of the distribution function. This is efficient as it reduces the size of the computational problem significantly. However, the plasma may still contain a vast number of particles: A solid density material may have a density of $n_e \sim 10^{24}\text{cm}^{-3}$ and a typical length scale of $l \sim 10\,\mu\text{m}$, leading to a total of $10^{15}$ particles. This is equivalent to $5 \times 10^4$ TB of memory in order to store the positions and velocities of the particles, which is well beyond reach for many modern computer systems. The PIC-method does therefore not model the real particles in the plasma, but instead uses super-particles to represent groups of particles which follow the same trajectories by maintaining the same charge to mass ratio as for the real particles.

Figure 4.1 gives an overview of the classical PIC-method. As was touched upon, the classical realization of the PIC-scheme starts from an initial setup of super-particles sampled from an initial distribution function and then consists of a main loop with four steps equivalent to advancing the state by one time step:

1. **Current deposition:** The currents needed for time advancement of the fields are calculated. The super-particles are associated with a shape factor, which describes how the current should be distributed over the grid points. This can allow for higher or-

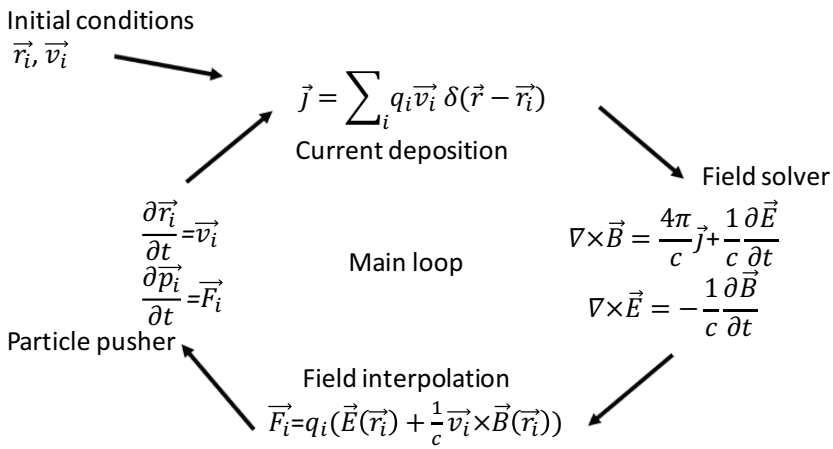


**Figure 4.1:** Overview of the main loop in the classical PIC-method.

der accuracy compared to if a simplistic view of the particles is adopted.

2. **Field solver:** The field solver advances the electromagnetic fields. There are several different techniques which may be used, for example FDTD (finite difference time domain) and spectral methods. In the former case, the fields are straightforwardly defined on points in real space whereas in the latter case, the fields are represented in Fourier-space and must be transformed to real space when calculating the Lorentz force. Spectral methods are dispersion free and are therefore of great benefit for applications to laser wakefield acceleration, where electrons are co-propagating with a laser pulse at a speed close to the speed of light.

3. **Field interpolation:** Before the particles can be advanced, field interpolation is performed to obtain the electromagnetic fields at the positions of the particles and consequently be able to evaluate the Lorentz force. As in the current deposition, the field interpolation is performed using a weighting scheme.

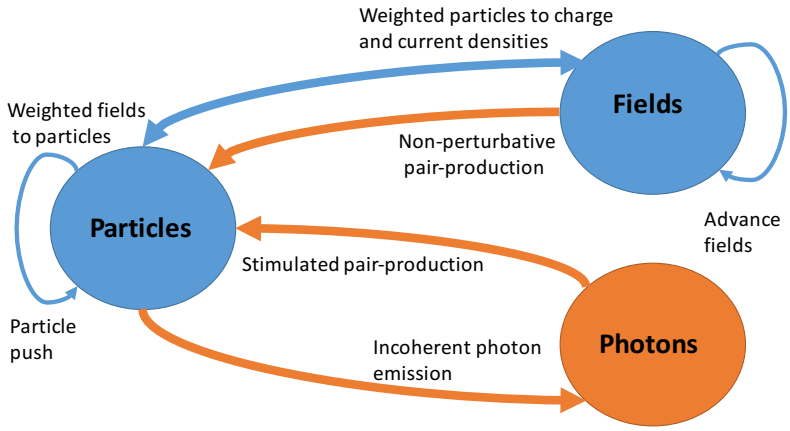


**Figure 4.2:** The classical PIC-method marked blue, with additions of QED-effects marked orange.

4. **Particle pusher:** The equations of motion for the super-particles are integrated. The method which is used to advance the positions of the particles is known as the particle pusher. The Boris pusher [39] is one of the most common particle pushers, which is a leap-frog method; commonly used because of its excellent long term accuracy.

The PIC-method renders itself extensible, incorporating new physics, through modules that are executed during different steps of the main loop. This may for example include modules for ionization, or, in the strongly relativistic regime, QED-effects. QED-effects are for example important in the study of X-ray wakefield acceleration in Paper C. Modular extensions of PIC-codes to include QED-effects are described in Gonoskov *et al* [20]. Figure 4.2 indicates the addition of QED-effects to the classical PIC-method. In this case, photons and positrons are added as plasma species, with emission events and pair-creation modelled using statistical routines based on QED-rates. Whereas the addition of positrons is conceptually straightforward, the addition of photons means

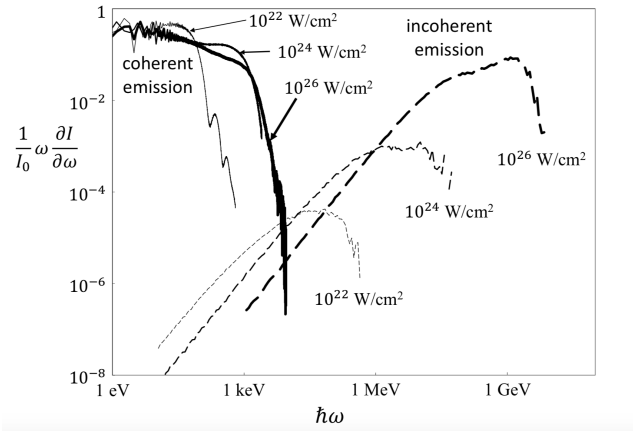


**Figure 4.3:** Spectra of coherent and incoherent emission. The figure is reprinted from [20].

that there is a dual representation of light: on one hand as the $\vec{E}$, $\vec{B}$ fields and on the other hand as particles. The possibility to split light into these two categories relies on that the radiation spectrum for a particle can be divided into a coherent part with low energy photons, which can be represented as fields, and an incoherent part with high energy photons for which the particle description is necessary. This is illustrated in Figure 4.3, which shows the spectra for coherent and incoherent radiation in a simulation of laser-plasma interaction in the RES-regime. This possibility is an important reason for the success and feasibility of simulations of relativistic laser plasma interaction as the typical frequency for photon emission grows as $\omega_c = 3eH_{\text{eff}}\gamma^2/2m_e c$, where $H_{\text{eff}}$ is the efficient magnetic field, which otherwise would need to be resolved using a very fine grid already for moderate $\gamma$.

## 4.1 PIC- versus continuum methods

Continuum methods [40] discretize the distribution function on a grid encompassing both the spatial dimensions and momentum dimensions, i.e. on a grid of dimension $2D$ instead of $D$ as in the PIC-case, where $D$ is the number of spatial dimensions. The PIC-method therefore has the advantage of using a smaller grid, which is computationally less costly. Although, the PIC-method is successful for numerical modelling of a

majority of problems in laser plasma interaction, there are a few: Where the sampling of the distribution function provides poor resolution of necessary regions of phase space with low density, for which a continuum approach to the Vlasov-Maxwell system of equations is more successful.

To estimate which one of the two approaches which is most useful [41] one may first note that in both methods, it is necessary for the spatial grid to resolve the Debye length $\lambda_D$. The number of spatial grid points therefore scales as $N_x^D = (L/\Delta x)^D$ where $\Delta x \sim \lambda_D$ and $L$ is a typical length scale for the problem. The relative performance can be estimated by the number of grid points used by the continuum solver in relation to the number of particles in the PIC-method : $N_{\text{continuum}}/N_{\text{PIC}}$. $N_{\text{continuum}}$ is estimated by $(L/\Delta x)^D N_p^D$, where $N_p$ is a typical number of points to resolve the momentum space dimension. For the PIC-method: $N_{\text{PIC}} = g_p(L/\Delta x)^D$ where $g_p$ is the number of particles per cell. Consequently $N_{\text{continuum}}/N_{\text{PIC}} = g_p^{-1} N_p^D$. For applications where a small number of particles per cell can be used, e.g. laser wakefield acceleration, the PIC-approach clearly has an advantage, whereas continuum methods are more favourable for the study of problems such as shock acceleration or instability growth where a higher number of particles per cell is needed. In summary, continuum methods are preferable if $g_p > N_p^D$, which shows that they are more competitive for low dimensional systems.

A number of approximations have been made in reaching the comparison in the previous paragraph: Firstly, $g_p$ is affected by factors such as the shape function used in the PIC-code, and the order of accuracy for the method used by the continuum solver also plays a role, both with regard to the number of needed grid points and the computational cost per grid point to take one time step. However, one may still argue that $N_{\text{continuum}}/N_{\text{PIC}}$ is proportional to the relative competitiveness. On the other hand, if it would be possible to use an adaptive mesh [42] which limited the number of grid points, by only applying high resolution in regions where it is needed, it could be possible to limit the unfavourable scaling for continuum methods with the dimension of the problem. Figure 4.4 shows the representation of a distribution function resulting from the interaction of a laser with a plasma using an adaptive grid. The grid consists of five levels of different coarseness, with higher resolution limited to regions that carry significant information. Benefits from the use of an adaptive mesh is treated further in Paper B.

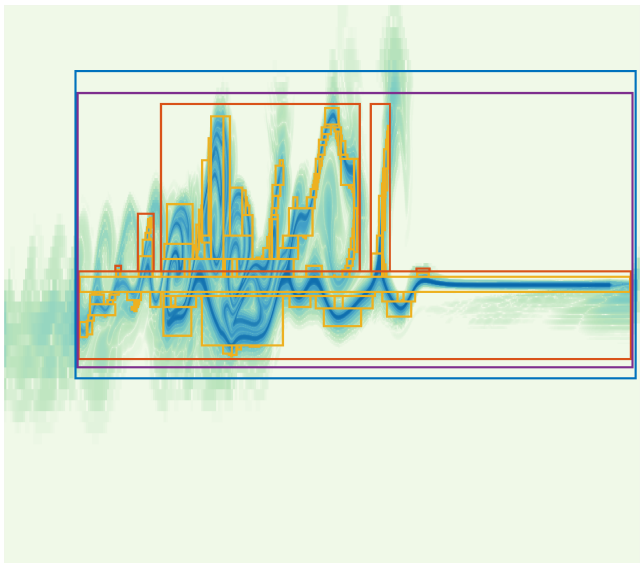

**Figure 4.4:** Distribution function represented on an adaptive mesh. By only applying high resolution in regions carrying significant information, it is possible to mitigate parts of the additional costs due to the momentum space grid in the continuum approach compared to in the PIC-method.

# Chapter 5

# Summary of papers

## Paper 1

**Vlasov modelling of laser-driven collisionless shock acceleration of protons**

In this paper, we implement and use continuum methods to solve the Vlasov-Maxwell system of equations in two dimensions (one spatial and momentum dimension). We investigate the interaction between the TNSA and shock acceleration mechanisms. In particular we study the effect of using a layered target, where the shock is launched in a front layer with light ions and then continues through a heavy ion backside. This leads to a removal of the TNSA contribution to the spectrum and increases the energy of the shock accelerated ions slightly.

*My contribution to this paper was to implement the code, run the simulations and to write the paper.*

## Paper 2

**Relativistic Vlasov-Maxwell modelling using finite volumes and adaptive mesh refinement**

In this paper, we present a block structured adaptive finite volume code that solves the Vlasov-Maxwell system in one spatial and momentum dimension. Adaptive mesh refinement may be one way to limit the unfavourable scaling of the computational cost with the dimension of the problem for continuum methods compared to in the PIC-method. We benchmark the solver and demonstrate speed-ups of the order 7x compared to if a fixed grid would have been used.

*My contribution to this paper was to implement the code, run the simulations and to write the paper.*

## Paper 3

**Prospects and limitations of wakefield acceleration in solids**

In this paper we investigate the effects of using a coherent X-ray pulse to drive wakefield acceleration in solid materials. We verify scalings based on similarity theory, leading to ultra-short electron and photon bunches. Furthermore, we demonstrate that photons are emitted with comparable energies to the accelerated electrons, already at moderate relativistic intensities $a_0$, making X-ray wakefield accelerators a promising source of high energy photons.

*My contribution to this paper was to run the simulations and to write the paper.*

# Bibliography


[1] T. H. Maiman, *Stimulated optical radiation in ruby*, Nature 187, 493-494.

[2] D. Strickland, G. Mourou, *Compression of amplified chirped optical pulses*, Optics Communications 56, 3, 219-221, 1985.

[3] Vulcan: `www.clf.stfc.ac.uk`.

[4] BELLA: `http://www2.lbl.gov/publicinfo/newscenter/features/2008/apr/af-bella.html`.

[5] XCELS: `www.xcels.iapras.ru`.

[6] J. M. Dawson, *Particle simulation of plasmas*, Rev.Mod. Phys., 55, 2, 403-447, 1983.

[7] C. K. Birdsall, A. B. Langdon, Plasma Physics via Computational Simulation, McGraw-Hill, 1985.

[8] ELI: `www.eli-laser.eu`.

[9] C. Z. Cheng, G. Knorr, *The integration of the Vlasov equation in configuration space*, J. Comp. Phys. 22, 3, 330-351, 1976.

[10] T. Tajima, J. M. Dawson, *Laser electron accelerator*, Phys. Rev. Lett., 43, 4, 267-270, 1979.

[11] W. P. Leemans, B. Nagler, A. J. Gonsalves, C. Toth, K. Nakamura, C. G. R. Geddes, E. Esarey, C. B. Schroeder, S. M. Hooker, *GeV electron beams from a centimetre-scale accelerator*, Nature Phys., 2, 696-699, 2006.

[12] V. I. Veksler, *Coherent principle of acceleration of charged particles* Proc. CERN Symp. of High Energy Accelerators and Pion Physics. Geneva, Switzerland, 1956.

[13] H. Daido, M. Nishiuchi, A. S. Pirozhkov, *Review of laser-driven ion sources and their applications*, Rev. Prog. Phys 75, 5, 056401, 2012.

[14] A. Macchi, M. Borgesi, M. Passoni, *Ion acceleration by superintense laser-plasma interaction*, Rev. Mod. Phys. 85, 2, 751-793, 2013.

[15] A. Macchi, *A superintense laser-plasma interaction theory primer*, Wiley, 2013.

[16] J. D. Jackson, *Classical Electrodynamics*, 3rd ed., Wiley, 1998.

[17] A. A. Vlasov. J. Phys. U.S.S.R., 9, 25, 1945.

[18] C. Cercignani, V. Gerasimenko, D. Petrina, *Many-particle dynamics and kinetic equations*, Mathematics and Its Applications, Springer, 1997.

[19] L. D. Landau, E. M. Lifshitz, The classical theory of fields. Elsevier, 1975.

[20] A. Gonoskov, S. Bastrakov, E. Efimenko, A. Ilderton, M. Marklund, I. Meyerov, A. Muraviev, A. Sergeev, I. Surmin, E. Wallin, *Extended particle-in-cell schemes for physics in ultrastrong laser fields: Review and developments*, Phys. Rev. E, 92, 2, 023305, 2015.

[21] F. Cattani, A. Kim, D. Anderson, M. Lisak, *Threshold of induced transparency in the relativistic interaction of an electromagnetic wave with overdense plasmas*, Phys. Rev. E 62, 1, 1234-1237, 2000.

[22] E. Siminos, M. Grech, S. Skupin, T. Schlegel, V. T. Tikhonchuk, *Effect of electron heating on self-induced transparency in relativistic-intensity laser-plasma interactions*, Phys. Rev. E 86, 056404, 2012.

[23] A. V. Korzhimanov, A. A. Gonoskov, A. V. Kim, A. M. Sergeev, *Interaction of relativistically strong electromagnetic waves with a layer of overdense plasma*, JETP 105, 4, 675-686, 2007.

[24] E. Siminos, M. Grech, B. Svedung Wettervik, T. Fülöp, *Kinetic and finite ion mass effects on the transition to relativistic self-induced transparency in laser-driven ion acceleration*, New Journal of Physics 19, 12, 123042, 2017.

[25] E. Esarey, C. B. Schroeder, W. P. Leemans, *Physics of laser-driven plasma-based electron accelerators*, Rev. Mod. Phys. 81, 3, 1229-1285, 2009.

[26] V. Malka, J. Faure, Gauduel, E. Y. A., Lefebvre, A. Rousse, and K. T. Phuoc, *Principles and applications of compact laser-plasma accelerators*, Nat. Phys. 4, 447, 2008.

[27] A. Pukhov, S. Gordienko, S. Kiselev, I. Kostyukov, *The bubble regime of laser-plasma acceleration: monoenergetic electrons and the scalability*, Plasma Physics and Controlled Fusion, 46, 12B, 2004.

[28] S. Gordienko, A. Pukhov, *Similarity for ultra-relativistic laser plasmas and the optimal acceleration regime*, arXiv:physics/0411099, 2004.

[29] T. Tajima, M. Cavenago, *Crystal x-ray accelerator*, Phys. Rev. Lett. 59, 1440, 1987.

[30] X. Zhang, T. Tajima, D. Farinella, Y. Shin, G. Mourou, J. Wheeler, P. Taborek, P. Chen, F. Dollar, B. Shen, *Particle-in-cell simulation of x-ray wakefield acceleration and betatron radiation in nanotubes*, Phys. Rev. Accel. Beams, 19, 10, 101004, 2016.

[31] A. A. Gonoskov, A. V. Korzhimanov, A. V. Kim, M. Marklund, A. M. Sergeev, *Ultrarelativistic nanoplasmonics as a route towards extreme-intensity attosecond pulses*, Phys. Rev. E 84, 4, 046403, 2011.

[32] A. A. Gonoskov, *Theory of relativistic radiation reflection from plasmas*, Physics of Plasmas 25, 013108, 2018.

[33] T. Blackburn, A. Gonoskov, M. Marklund, *Brilliant XUV radiation from laser-illuminated near-critical plasmas*, arXiv:1701.07268, 2017.

[34] A. Gonoskov, *Ultra-intense laser-plasma interaction for applied and fundamental physics*, Ph.D. thesis, Umeå University, 2013.

[35] B. Svedung Wettervik, A. Gonoskov, M. Marklund, *Prospects and limitations of wakefield acceleration in solids* Physics of Plasmas 25, 013107, 2018.

[36] F. Fiuza, A. Stockem, E. Boella, R. A. Fonseca, L. O. Silva, D. Haberberger, S. Tochitsky, C. Gong, W. B. Mori, C. Joshi, *Laser-Driven Shock Acceleration of Monoenergetic Ion Beams*, Phys. Rev. Lett. 109, 215001, 2012.

[37] S. S. Moiseev, R. Z. Sagdeev, *Collisionless shock waves in a plasma in weak magnetic fields*, Journal of Nuclear Energy Part C 5, 1, 32-47, 1963.

[38] B. Svedung Wettervik, T. C. DuBois, T. Fülöp, *Vlasov modelling of laser-driven collisionless shock acceleration of protons*, Physics of Plasmas, 23, 5, 053103, 2016.

[39] J. P. Boris, *Relativistic plasma simulation-optimization of a hybrid code*, Proceeding of Fourth Conference on Numerical Simulations of Plasmas, 1970.

[40] M. Shoucri, ed., *Eulerian codes for the numerical solution of the kinetic equations of plasmas*, Nova Science Publishers, New York, 2011.

[41] N. Besse, G. Latu, A. Ghizzo, E. Sonnendrücker, P. Bertrand, *A wavelet-MRA-based adaptive semi-Lagrangian method for the relativistic Vlasov-Maxwell system*, Journal of Computational Physics 227, 16, 7889-7916, 2008.

[42] J. Hittinger, J. Banks, *Block-structured adaptive mesh refinement algorithms for Vlasov simulation*, Journal of Computational Physics 241, 118-140, 2013.

[43] B. Svedung Wettervik, T. C. DuBois, E. Siminos, T. Fülöp, *Relativistic Vlasov-Maxwell modelling using finite volumes and adaptive mesh refinement*, The European Physical Journal D, 71, 6, 156-171, 2017.